Journal of the European Ceramic Society **9** (1992) 271–283

Revised Phase Equilibrium Relationships in the System Al_2O_3–ZrO_2–SiO_2

Maria Conceição Greca,* José Vitório Emiliano‡ & Ana Maria Segadães§

Departamento de Engenharia Cerâmica e do Vidro, Universidade de Aveiro, 3800 Aveiro, Portugal

(Received 27 June 1991; accepted 16 August 1991)

Abstract

Current research on the mechanical behaviour of ceramic matrices reinforced by zirconia particles, and on the processing of mullite–zirconia composites via reaction sintering, has brought about the need to update the phase diagram of the system Al_2O_3–ZrO_2–SiO_2, whose available version dates back to 1956.

In the present work selected compositions in this system were prepared from reagent-grade oxides, uniaxially pressed into 6 mm cylindrical pellets, fired at temperatures between 1550 and 1750°C for 6 to 24 h, water-quenched, and observed by X-ray diffraction and SEM, the composition of some of the phases identified being evaluated by EPMA. These experiments led to the relocation of the boundary curves neighbouring the ternary eutectic involving alumina, zirconia and mullite. This eutectic was found to occur between 1700 and 1710°C, a temperature significantly lower than previously reported, and at a composition c. *$11SiO_2 + 58Al_2O_3 + 31ZrO_2$ (wt%).*

Die gegenwärtige Forschung bezüglich des mechanischen Verhaltens von Zirkonoxid-Partikel verstärkten Keramik-Matrizes und bezüglich der Herstellungsverfahren von Mullit–Zirkonoxid-Verbunden über Reaktionssintern, erfordert die Überarbeitung des Phasendiagrammes des Systemes Al_2O_3–ZrO_2–SiO_2, dessen jetzige verfügbare Version auf das Jahr 1956 zurückgeht.

In dieser Arbeit wurden ausgewählte Zusammensetzungen dieses Systems aus reagenzienreinen Oxiden hergestellt, uniaxial zu zylindrischen Pellets mit 6 mm Durchmesser verpreßt, bei Temperaturen zwischen 1550 und 1750°C für 6 bis 24 h gebrannt, in Wasser abgeschreckt und mit Hilfe von Röntgendiffraktometrie und Rasterelektronenmikroskopie untersucht. Die Zusammensetzungen einiger der identifizierten Phasen wurden mittels Mikrosonde-Messungen bestimmt. Die Ergebnisse dieser Experimente führen zu einer Verschiebung der Grenzkurven in der Nähe des ternären Eutektikums aus Aluminiumoxid, Zirkonoxid und Mullit. Es wurde festgestellt, daß dieses Eutektikum zwischen 1700 und 1710°C auftritt, also bei einer erheblich tieferen Temperatur als ursprünglich berichtet, und bei einer Zusammensetzung von $11SiO_2 + 58Al_2O_3 + 31ZrO_2$ (Gew.%).

Des recherches en cours sur le comportement mécanique de matrices céramiques renforcées par des particules de zircone, ainsi que sur le traitement de composites mullite–zircone par frittage-réaction, ont mis en évidence la nécessité de réactualiser le diagramme de phase du système Al_2O_3–ZrO_2–SiO_2, dont la version disponible date de 1956.

On a préparé pour la présente étude, à partir d'oxydes grade réactif, des poudres de diverses compositions sélectionnées dans ce système. On les a pressées de façon uniaxiale selon des pastilles cylindriques de 6 mm, chauffées entre 1550 et 1750°C pendant 6 à 24 h, trempées à l'eau, et observées par diffraction RX et MEB, la composition de certaines phases identifiées étant évaluée par EPMA. Ces expériences conduisent à un repositionnement des courbes de séparation voisines de l'eutectique ternaire constitué par l'alumine, la zircone et la mullite. On montre que l'eutectique se situe entre 1700 et 1710°C, une température notablement inférieure à celle ultérieurement indiquée, et à une composition en %-masse d'environ $11SiO_2 + 58Al_2O_3 + 31ZrO_2$.

* Present address: MCT-Instituto Nacional de Tecnologia, Avenida Venezuela, 82–6° andar, 20081 Rio de Janeiro–RJ, Brazil.

‡ Present address: Universidade Federal de São Carlos, Departamento de Engenharia de Materiais, Cx.P. 676, 13560 São Carlos–SP, Brazil.

§ To whom correspondence should be addressed.

Journal of the European Ceramic Society 0955-2219/92/$5.00

1 Introduction

For a number of reasons mullite ($3Al_2O_3 . 2SiO_2$) has long been considered the silicate of the ceramists. Being the major constituent of most traditional clay-based ceramics, mullite has become more and more involved in advanced ceramics. From this point of view some of its most attractive characteristics are the low thermal expansion coefficient, low dielectric constant and high chemical stability. However, mullite's comparatively modest mechanical properties have hindered a few of its most promising applications and considerable efforts have been dedicated to improving them. During the past decade it was shown that the addition of zirconia particles enhances the mechanical characteristics of otherwise brittle matrices[1,2] which brought about new expectations for mullite-based ceramics, namely mullite–zirconia composites.

It is worth noting that the first references to composite materials in the Al_2O_3–ZrO_2–SiO_2 system date back to 1926, regarding zirconia additions to fusion-cast mullite refractories.[3] Although the zirconia additions were aimed at improving the manufacturing process, it was soon found that the refractory's resistance to chemical corrosion in the glass melting furnace had been greatly enhanced, which led to full-scale production of this type of material from the 1940s onwards.

An important contribution to the special appeal of mullite–zirconia composites came about when Claussen & Jahn[4] introduced the reaction-sintering concept, a seemingly straightforward mechanism by which zirconia-toughened mullite materials can be produced from the reaction between alumina and zircon ($ZrSiO_4$) at temperatures around 1450°C.

Naturally research work such as this calls for the phase diagram of the system Al_2O_3–ZrO_2–SiO_2. The original version, reproduced in Fig. 1, is due to Budnikov & Litvakovskii (Ref. 5, Fig. 772) and dates back to 1956. However, since the 1960s new, more accurate, versions of the phase diagrams of the binary systems involved[5,6] have been reported (Fig. 2), and these clearly show that the available ternary phase diagram needs to be updated.

2 Experimental Procedure

In the present work selected compositions were prepared using alumina powder (Alcoa CT 3000), 90% of which was below 2 μm in size, with purity better than 99·08 wt% and BET specific surface area of 7·34 m^2/g, zircon powder containing 32·9 wt% silica and 65·9 wt% zirconia, with an average grain size of 1·35 μm and a BET specific surface area of 6·0 m^2/g, and colloidal silica (BDH Chemicals Ltd, UK) with a purity better than 99·00%.

The appropriate amounts of the reactants were dry-mixed for 30 min in a Glen–Creston mixer–miller, and uniaxially dry-pressed into 6 mm cylindrical pellets using a hard-steel die, under a pressure

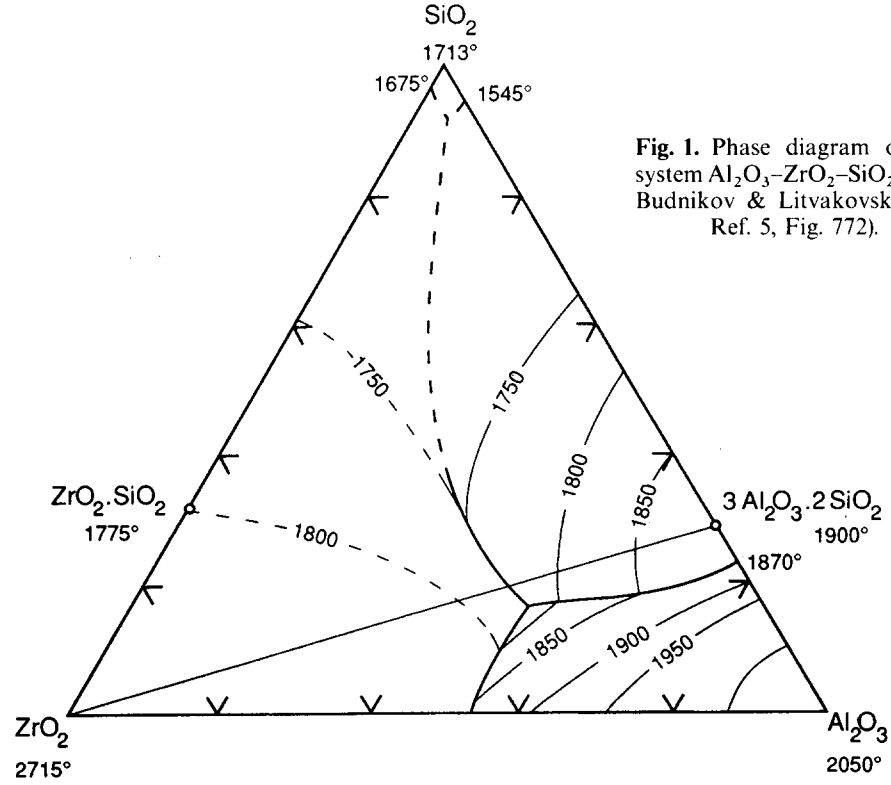

Fig. 1. Phase diagram of the system Al_2O_3–ZrO_2–SiO_2, after Budnikov & Litvakovskii (see Ref. 5, Fig. 772).

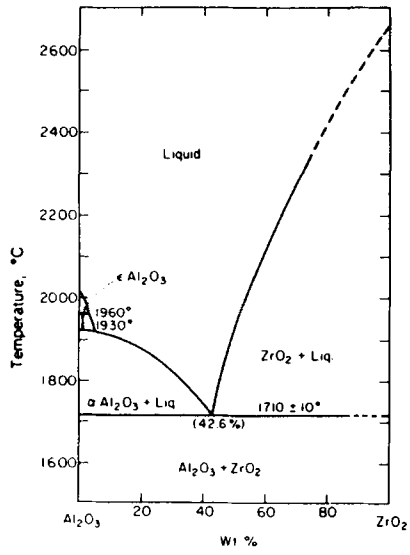

(a)

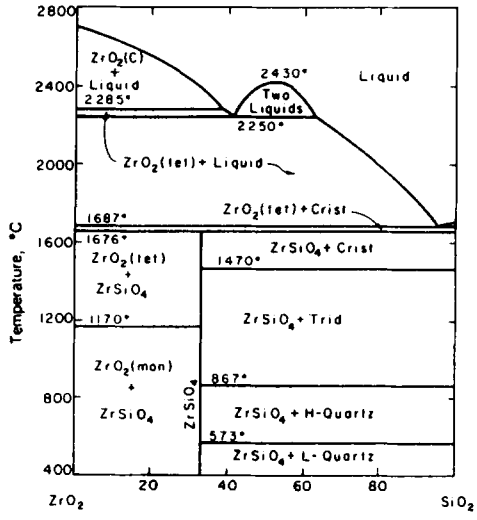

(b)

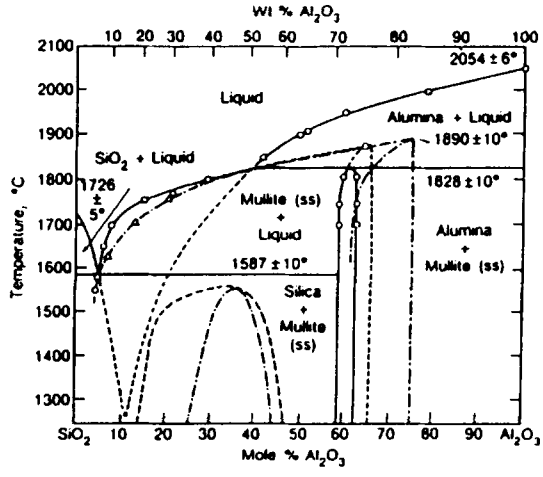

(c)

Fig. 2. Phase diagrams of the binary systems (a) Al_2O_3–ZrO_2, after Cevales (see Ref. 5, Fig. 4377); (b) ZrO_2–SiO_2, after Butterman & Foster (see Ref. 5, Fig. 2400); and (c) Al_2O_3–SiO_2, after Pask (see Ref. 6).

of ~100 MPa. Each pellet was then wrapped in platinum foil, lowered into a molybdenum wound vertical tube furnace held at the chosen soaking temperature, ranging from 1550 to 1750°C, for 6 to 24 h , and water-quenched. Temperatures were measured with Pt–10% Rh/Pt–30% Rh thermocouples.

To guarantee that equilibrium had been established, particularly in those samples fired at lower temperatures, the same composition was held for successively longer times at the particular temperature, until the phase assemblage observed did not change any further. The shortest time required to attain this was then considered to be enough to establish the equilibrium state. Naturally samples fired at higher temperatures, most of which containing a liquid phase, needed shorter firing times.

The fired samples were then prepared for X-ray powder diffraction and/or SEM analysis on epoxy-mounted polished surfaces. The compositions of some of the phases thus identified were evaluated by EPMA. Sample charging in SEM and EPMA was prevented by carbon coating. EPMA was carried out using elemental standards, the oxygen being calculated by difference (semi-quantitative analysis).

Table 1 gathers all the relevant data thus obtained. This table is constructed in the traditional way for phase equilibrium studies in ceramic oxide systems, i.e. only the major phases present are listed, those present in only trace amounts are shown with '(tr)' added, and when they do not represent true equilibrium they are shown in parentheses. When some details could not be determined beyond doubt during microscope examination, due to the poorly defined microstructure, the particular phase is listed as being 'undefined'.

3 Results and Discussion

3.1 Initial melting temperature in the alumina–zirconia–mullite triangle

Because of the incongruent melting of mullite[6] there is the possibility of a ternary peritectic point for this triangle, which would lie outside it, i.e. within the alumina–zirconia–silica triangle. Assuming that the invariant point for the mullite–zirconia–silica triangle is a eutectic, as proposed by the diagram of Budnikov & Litvakovskii (Fig. 1), if the ternary invariant point of the alumina–zirconia–mullite triangle is a peritectic, the temperature on the boundary line between the mullite and zirconia primary phase fields will continuously drop from this peritectic to the eutectic between zirconia,

Table 1. Selected compositions and phases identified in the system Al_2O_3–ZrO_2–SiO_2

Sample number	*Composition (wt%)*			*Temperature (°C)*	*Time (h)*	*Phases identified*		*Composition of amorphous/liquid phase*			*Composition of second crystalline phase*		
	Al_2O_3	SiO_2	ZrO_2			*XRD*	*SEM*	Al_2O_3	SiO_2	ZrO_2	Al_2O_3	SiO_2	ZrO_2
1	70·00	10·00	20·00	1 680	9	A + Z	A + Z + amorphous phase	74·56	25·41	—			
				1 700	9	A + Z	A + Z + amorphous phase						
				1 715	6·5	A + Z	A(+Z) + undefined	75·29	24·67	—			
				1 735	6·5	A + Z	A + devitrified liquid (Z)						
2	67·00	13·00	20·00	1 680	9	A + Z	A + Z + amorphous phase	75·16	24·81	—			
				1 700	9	A + Z	A + Z + amorphous phase						
				1 715	6·5	A + Z	A(+Z) + undefined	74·55	25·41	—			
				1 735	6·5	A + Z	A + devitrified liquid (Z)						
3	60·00	20·00	20·00	1 550	24	Z + M + A	Z + A + undefined						
				1 600	24	Z + M + A	Z + A + undefined						
				1 650	24	Z + M + A	Z + A + undefined						
				1 700	24	Z + M(+A)	Z + M + liquid	36·22	41·78	21·95			
				1 750	24	Z + A	M + devitrified liquid (Z)						
4	60·00	15·00	25·00	1 550	24	Z + M + A	Z + M + A						
				1 600	24	Z + M + A	Z + M + A						
				1 650	24	Z + M + A	Z + M + A						
				1 700	24	Z + M + A	Z + M + A				75·48	23·51	0·96
				1 750	24	M + A	M + devitrified liquid (Z)	55·59	20·64	23·71			
5	60·00	10·00	30·00	1 550	24	Z + M + A	Z + A + undefined						
				1 600	24	Z + M + A	Z + A + undefined						
				1 650	24	Z + M + A	Z + M + A						
				1 700	24	Z + M + A	Z + M + A						
				1 750	24	Z + A	A + devitrified liquid (Z)						
6	58·72	21·28	20·00	1 680	9	Z + M	Z + undefined						
				1 700	9	Z + M	Z + undefined						
				1 715	6·5	Z + M	Z + M(+A + liquid)				79·03	20·94	—
				1 735	6·5	Z + M	M + devitrified liquid (Z)				78·60	21·40	—
7	55·00	25·00	20·00	1 680	9	Z + M	Z + undefined						
				1 700	9	Z + M	Z + undefined + devitrified liquid						
				1 715	6·5	Z + M	Z(tr) + M + devitrified liquid (Z)				77·50	22·50	—
				1 735	6·5	Z + M	M + devitrified liquid (Z)				79·60	20·40	—
8	55·00	20·00	25·00	1 550	24	Z + M + A	Z + undefined						
				1 600	24	Z + M + A	Z + undefined						
				1 650	24	Z + M + A	Z + M + undefined						
				1 700	24	Z + M + A	Z + M + undefined						
				1 750	24	Z + M	Z + M + devitrified liquid (Z)						
9	55·00	15·00	30·00	1 550	24	Z + M + A	Z + M + A						
				1 600	24	Z + M + A	Z + M + A						
				1 650	24	Z + M + A	Z + M + A						
				1 700	24	Z + M + A	Z + M(+A)						
				1 750	24	Z + A	Z(+A) + devitrified liquid (Z)	55·70	19·97	24·32			

10	55·00	10·00	35·00	1 550	24	Z + M + A	Z + A + undefined						
				1 600	12	Z(+ M) + A	Z + A + undefined	72·65	24·98	2·31			
				1 600	18	Z + M + A	Z + A + undefined	73·08	25·00	1·88			
				1 650	24	Z + M + A	Z + M + A						
				1 700	24	Z + M + A	Z + M + A						
				1 750	24	Z + A	Z(+ A) + devitrified liquid (Z)						
11	50·00	20·00	30·00	1 550	24	Z + M + A	Z + undefined						
				1 600	24	Z + M + A	Z + undefined						
				1 650	24	Z + M + A	Z + undefined						
				1 700	24	Z + M + A	Z + M + undefined						
				1 750	24	Z + M	Z + M + liquid	54·31	21·76	23·88	75·52	24·26	0·16
12	50·00	15·00	35·00	1 550	24	Z + M + A	Z + M + A						
				1 600	24	Z + M + A	Z + M + A						
				1 650	24	Z + M + A	Z + M + A						
				1 700	24	Z + M + A	Z + M(+ A)						
				1 750	24	Z + M	Z + M + devitrified liquid (Z)	54·86	19·97	25·12			
13	50·00	10·00	40·00	1 550	24	Z + M + A	Z + A + undefined						
				1 600	24	Z + M + A	Z + M + A				76·40	23·60	—
				1 650	24	Z + M + A	Z + M + A						
				1 700	24	Z + M + A	Z + M + A						
				1 750	24	Z + A	Z(+ A) + devitrified liquid (Z)						
14	46·00	17·38	36·62	1 680	9	Z + M(tr)	Z(+ A) + amorphous phase						
				1 700	9	Z + M(tr)	Z(+ A) + amorphous phase						
				1 715	6·5	Z + M(tr)	Z + M + devitrified liquid (Z)				78·40	21·60	—
				1 735	6·5	Z + M(tr)	Z + devitrified liquid (Z + A)	51·07	21·84	27·04			
15	40·00	20·00	40·00	1 550	24	Z + M	Z + M + undefined						
				1 600	24	Z + M	Z + M + undefined						
				1 650	24	Z + M	Z + M + undefined						
				1 680	9	Z + M(tr)	Z + M + amorphous phase						
				1 700	9	Z + M(tr)	Z + M + devitrified liquid (Z)						
				1 700	24	Z + M	Z + M + liquid						
				1 715	6·5	Z + M(tr)	Z + M + devitrified liquid (Z)				78·35	21·65	—
				1 735	6·5	Z + M(tr)	Z + devitrified liquid (Z)	50·32	26·88	22·75			
				1 750	24	Z + M	Z + liquid						
16	40·00	15·00	45·00	1 550	24	Z + M	Z + M				77·60	22·40	—
				1 600	24	Z + M	Z + M						
				1 650	24	Z + M	Z + M						
				1 700	24	Z + M	Z + M						
				1 750	24	Z + M	Z + M + liquid						
17	40·00	10·00	50·00	1 550	24	Z + M + A	Z + M + A						
				1 600	24	Z + M + A	Z + M + A						
				1 650	24	Z + M + A	Z + M + A						
				1 700	24	Z + M + A	Z + M + undefined						
				1 750	24	Z(+ A)	Z + M + liquid						

A = alumina; M = mullite; Z = zirconia; (tr) = trace.

mullite and silica (Alkemade's theorem). Then the temperature should also drop from the binary eutectic at $1710 \pm 10°C$ in the Al_2O_3–ZrO_2 system, along the boundary between the alumina- and zirconia-phase fields, towards the ternary invariant point, and all temperatures along both boundaries will have to be lower than $1710 \pm 10°C$.

If the ternary invariant point relating alumina, zirconia and mullite is of the eutectic type, then a temperature maximum will occur on the boundary between the mullite and zirconia primary phase fields, where it crosses the Alkemade line, dropping from there to each side, towards the two eutectics, and that temperature maximum can be any value above or below the binary eutectic (the only restriction is relative to the ternary eutectic temperatures, which have to be lower than the maximum).

In the binary systems that form the outer edges of the alumina–zirconia–mullite compatibility triangle the invariant points occur at $1828 \pm 10°C$ in the Al_2O_3–SiO_2 system and at $1710 \pm 10°C$ in the Al_2O_3–ZrO_2 system (Fig. 2). Therefore, whether the ternary invariant point is of the eutectic or the peritectic type, it must occur at a temperature lower than $1710 \pm 10°C$. And, indeed, simple naked eye observation of all samples fired above 1700°C suggests the presence of an abundant liquid phase: these samples show significant shrinkage, are shiny and have rounded contours.

Most of the SEM observed microstructures seem to present a continuous phase around the crystalline grains (the usual appearance of a liquid phase), even at temperatures below 1700°C (Fig. 3). At these lower temperatures, however, this phase is not clearly defined and sometimes is detected by X-ray diffraction. EPMA showed that its chemical composition is close to mullite. Given that the samples were prepared with alumina and zircon (and silica when needed), the reaction-sintering mechanism should prevail, and it has been shown[7] that when the reaction between zircon and alumina is carried out there is a time when zirconia is detected by X-ray diffraction (decomposition of zircon has occurred), alumina peaks decrease, but no silica or mullite are found. It is presumed that silica underwent reaction to form non-crystalline mullite. It might thus be concluded that this continuous phase is amorphous mullite and not a liquid phase, and is listed as such in Table 1.

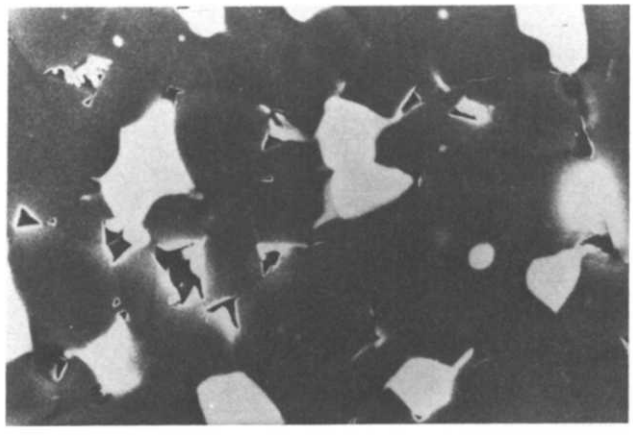

Fig. 3. Microstructure of the sample containing $67Al_2O_3 + 13SiO_2 + 20ZrO_2$, at 1700°C, in the alumina primary phase field, showing alumina (black) and zirconia (white) grains smeared by thin films of an amorphous phase.

The compositions of all the phases identified as mullite (crystalline or otherwise), which average $78{\cdot}6\ Al_2O_3 + 21{\cdot}4\ SiO_2$ (wt%), are higher in alumina than the stoichiometric $71{\cdot}8\ Al_2O_3 + 28{\cdot}2\ SiO_2$ (wt%). This agrees with mullite's reported high-temperature solid-solution range,[6] up to ~83 wt% Al_2O_3. Taking that average composition as the extreme of the mullite solid solution, the Alkemade line between zirconia and mullite is rotated towards lower silica contents and is replaced by a fan-like zirconia-mullite (solid solution) compatibility region. Hence the liquid phase presumed in samples like numbers 6, 14 and 16 (originally prepared to be on that Alkamade line) at temperatures below 1700°C adds nothing to the invariant temperature sought (i.e. for the alumina–zirconia–mullite triangle). In fact, due to the change in composition of mullite solid solution, those samples really lie in the compatibility triangle zirconia–mullite–silica, where liquid phase is supposed to form at 1550°C. It is, therefore, not surprising that such samples contain a liquid phase below 1700°C. In samples located well inside the compatibility triangle zirconia–mullite–silica, like sample numbers 7, 11 and 15, the presence of a liquid phase at 1700°C is readily identified. In samples actually belonging to the alumina–zirconia–mullite triangle no liquid phase could clearly be identified at this temperature, but their macroscopic appearance definitely changes when temperature rises above that value.

In the microstructures of all samples fired at higher temperatures (1735 and 1750°C) the well-developed liquid (glassy) phase sometimes contains a great number of dendritic zirconia crystals, presumed to have precipitated from the liquid phase during the quenching process; this is shown as 'devitrified liquid' in Table 1. In such cases, like sample number 4 at 1750°C, the interstitial liquid composition, as determined by EPMA, is silica-enriched and can not be taken as representative of the actual liquid-phase composition.

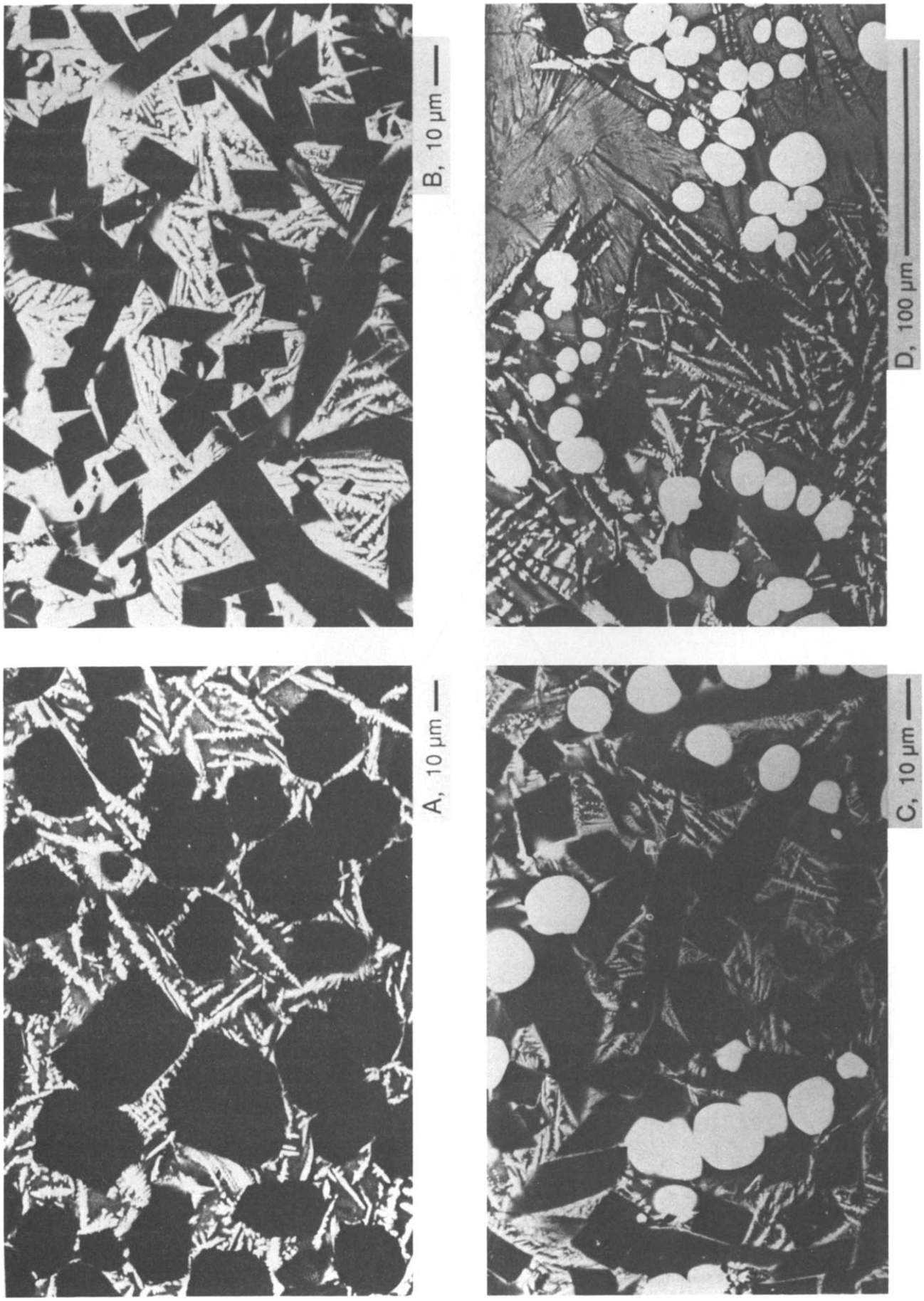

Fig. 4. Representative microstructures observed in the samples investigated: A, $67Al_2O_3 + 13SiO_2 + 20ZrO_2$, at 1735°C, showing alumina primary grains in a devitrified silica-rich matrix with zirconia dendrites; B, $55Al_2O_3 + 25SiO_2 + 20ZrO_2$, at 1735°C, showing mullite primary grains in a devitrified matrix with zirconia dendrites; C, $40Al_2O_3 + 20SiO_2 + 40ZrO_2$, at 1735°C, showing zirconia and mullite grains in a devitrified matrix with zirconia dendrites; D, $46Al_2O_3 + 17{\cdot}38SiO_2 + 36{\cdot}62ZrO_2$, at 1735°C, showing zirconia primary grains and residual unreacted alumina grains in a devitrified matrix with zirconia dendrites and mullite needles.

Indeed, it was found that the liquid phase tends to devitrify easily during quenching, with crystallization of zirconia dendrites and alumina and/or mullite needles, and also that unreacted alumina grains can sometimes be found. These apparently non-equilibrium situations can be readily identified and the samples in question should be regarded as containing only a primary phase in equilibrium with a liquid. Such non-equilibrium phases, when identified in the microstructure, are placed in parentheses in Table 1.

In all these samples, and when present, the zirconia grains appear as rounded, bright white crystals, the dark grey mullite grains develop a lath-like shape and the almost black alumina crystals present polygonal contours (Fig. 4). In the microstructures of the samples fired at 1700 and 1715°C, although a liquid phase is not readily identified, the grain morphology of the crystalline phases still suggests a growth mechanism in the presence of significant amounts of a liquid phase, as is consistently observed in the microstructures of samples fired at higher temperatures. The micrographs in Figs 3 and 4 illustrate these various features.

This reasoning places the ternary invariant point relating alumina, zirconia and mullite at a temperature between 1700 and 1715°C. Given that the binary eutectic in the Al_2O_3–ZrO_2 system occurs at 1710°C, the ternary invariant point must occur below 1710°C, a temperature significantly lower than the value reported by Budnikov & Litvakovskii (see Ref. 5).

3.2 Location of boundary curves between primary-phase fields

Some samples presented microstructures containing well-developed grains of a primary phase surrounded by liquid, together with an interstitial phase formed by numerous small zirconia and mullite crystals, too coarse to be just the result of devitrification during quenching. This morphology suggests a eutectic (simultaneous) crystallization of these two phases, and the composition of the liquid phase that accompanies them should thus be located on the

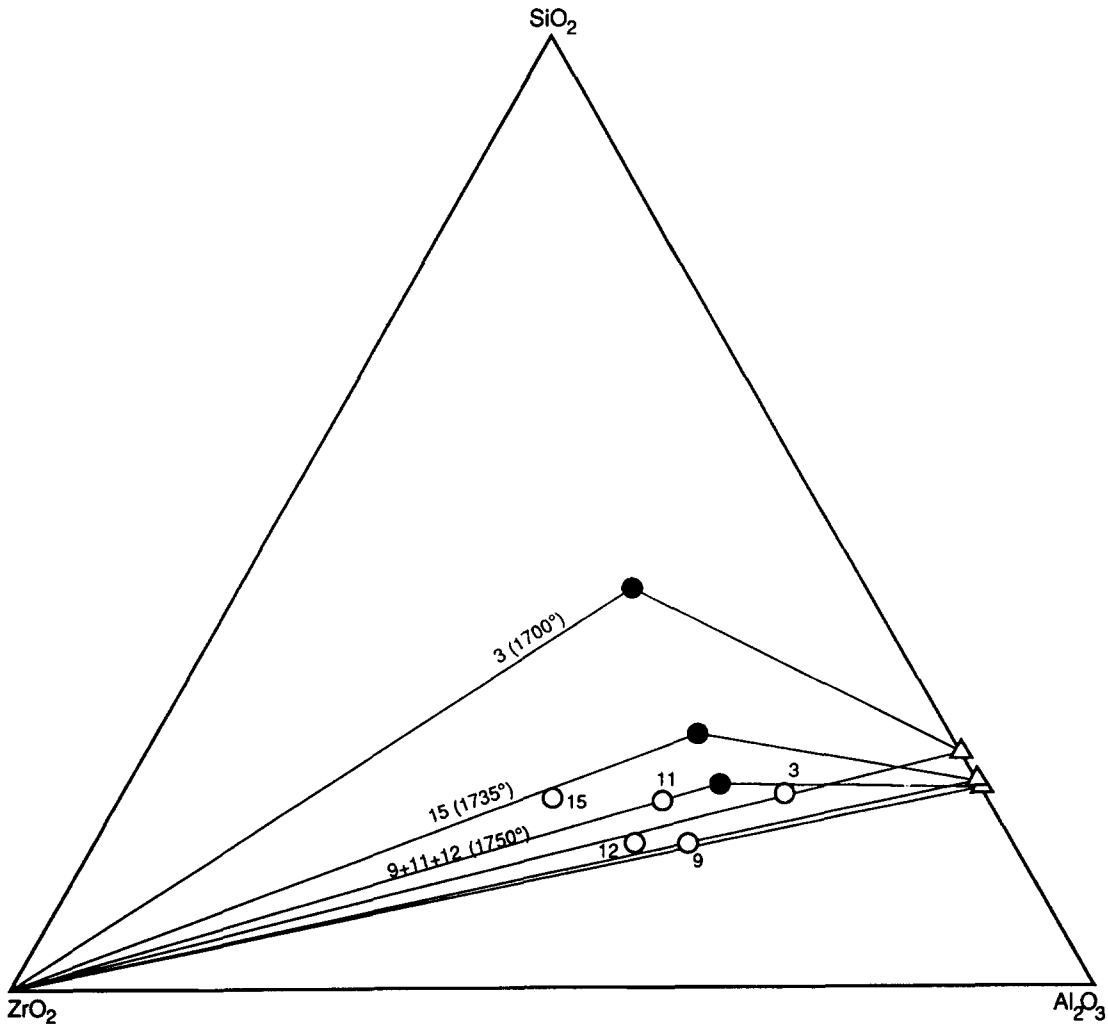

Fig. 5. Relationships between the starting compositions of selected samples (○) and those of the corresponding liquid phase (●) and mullite (△) in equilibrium at the temperatures shown.

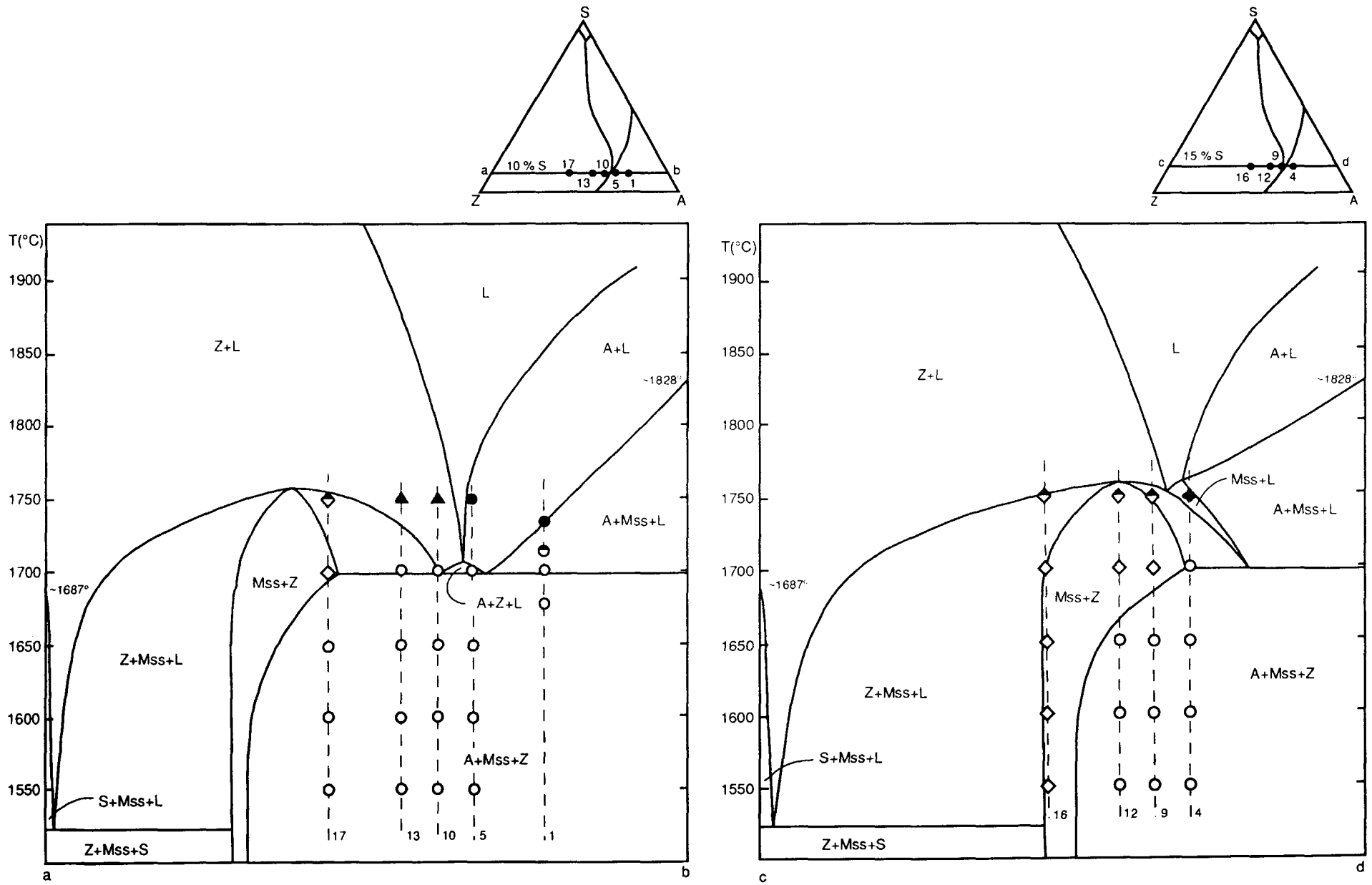

(a)

Fig. 6. Isoplethal sections at (a) constant 10 and 15 wt% SiO_2, (b) constant 20 wt% SiO_2 and 40 wt% Al_2O_3, and (c) constant 50, 55 and 60 wt% Al_2O_3. ○, ◇, △, Three solid phases; ◓, ◈, two solids + liquid; ●, ◆, ▲, one solid + liquid.

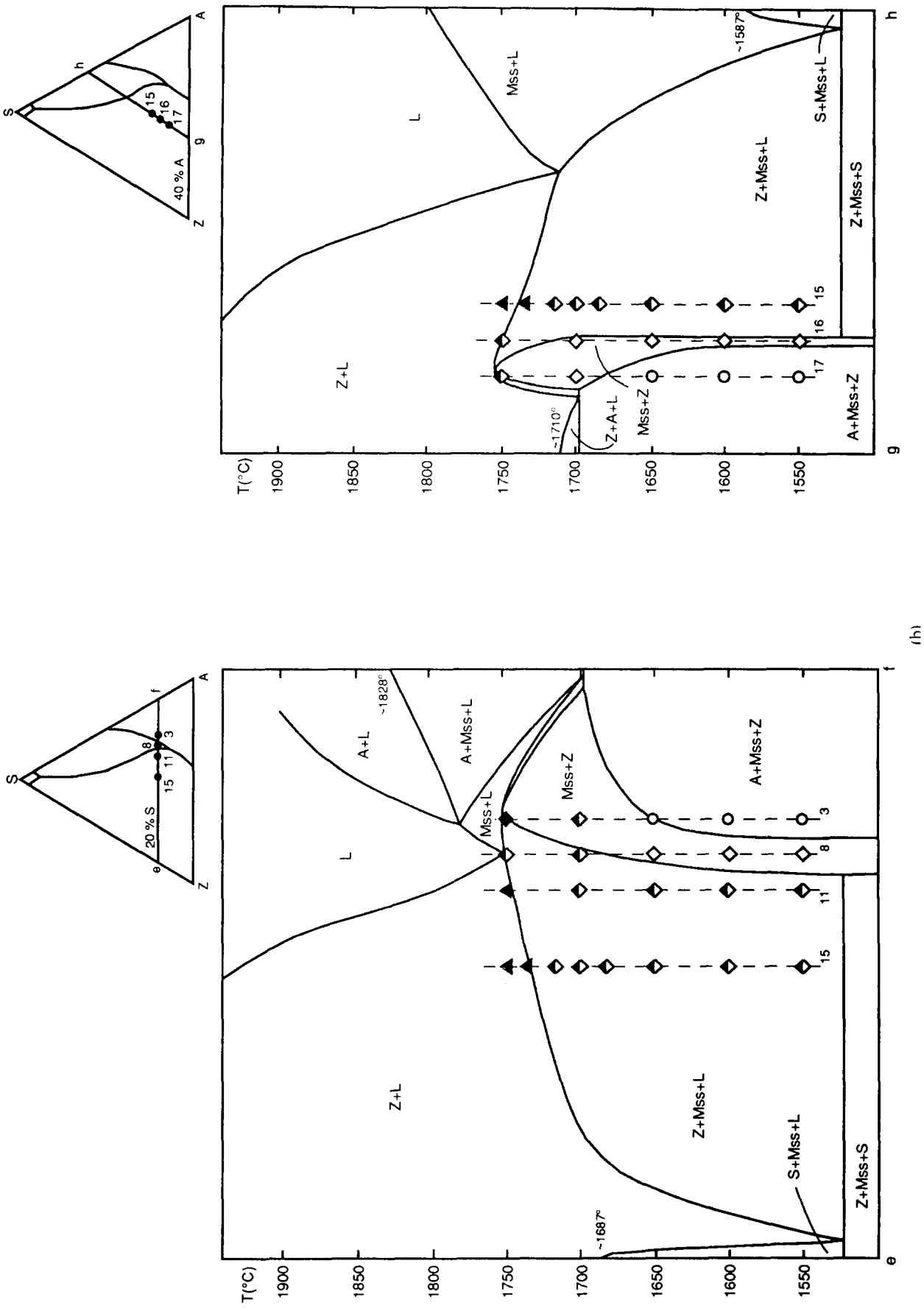
S
A
Z
h
g
15
16
17
40 % A
T(°C)
1900
1850
1800
1750
1700
1650
1600
1550
L
Mss+L
Z+L
Z+Mss+L
S+Mss+L
Z+Mss+S
~1587°
~1710°
Z+A+L
Mss+Z
A+Mss+Z
e
f
3
8
11
20 % S
A+L
~1828°
A+Mss+L
~1687°
(h)

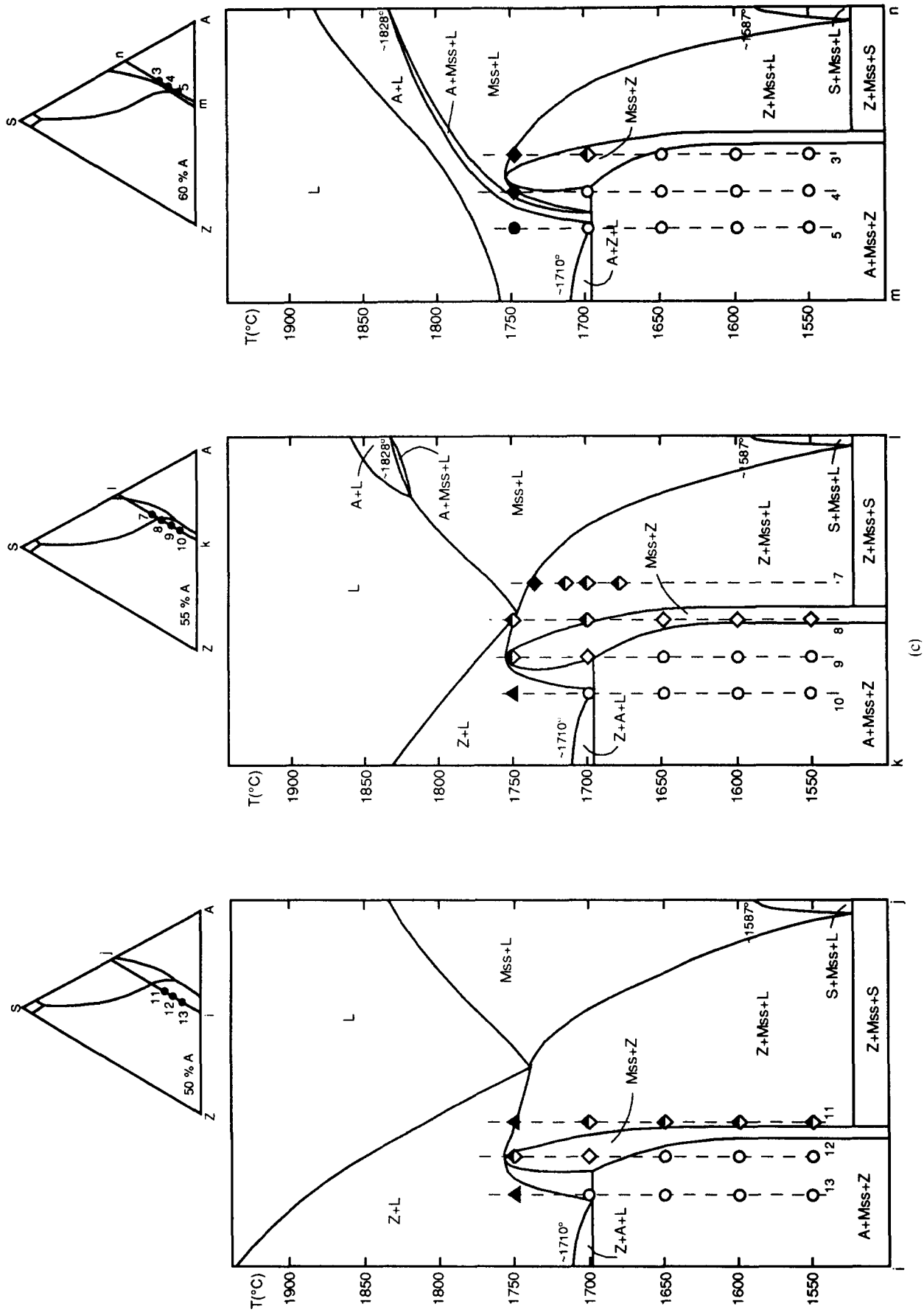
S
A
Z
50 % A
55 % A
60 % A
T(°C)
1900
1850
1800
1750
1700
1650
1600
1550
L
Z+L
A+L
A+Mss+L
Mss+L
Mss+Z
Z+Mss+L
S+Mss+L
Z+Mss+S
A+Mss+Z
Z+A+L
A+Z+L
~1828°
~1587°
~1710°
i
j
k
l
m
n
(c)

boundary curve between the corresponding primary-phase fields. The liquid phases in such samples, when fired at the same temperature, were found to have the same composition, within experimental accuracy (see Table 1), and were therefore used to locate temperature/composition points on that boundary curve. Figure 5 shows the starting compositions of those selected samples, and the compositions of the equilibrium liquid phase and mullite produced at the temperatures shown, obtained by EPMA. This figure was aimed at helping visualize the compatibility relationships. Data points are thus enlarged and exaggerated for the sake of clarity.

These liquid compositions are all in the zirconia–mullite–silica compatibility triangle and the corresponding temperatures along the boundary curve between the zirconia and mullite primary-phase fields decrease toward the silica apex of the diagram. However, they start higher than the temperature found for the ternary invariant point in the zirconia–mullite–alumina compatibility triangle, as high as 1750°C for the liquid phase in samples 9, 11 and 12. Hence there is a temperature maximum on that boundary curve, where it crosses the zirconia–mullite (solid solution) compatibility region, and the latter invariant point is of the eutectic type.

3.3 Proposed phase diagram for the system Al_2O_3–ZrO_2–SiO_2

The experimental data gathered were used to construct the isoplethal sections presented in Fig. 6. The overall shape of these sections, formerly constructed from Fig. 1, was adapted to fit the experimental results and, from them, the arguments discussed and the relevant information extracted from the binary systems (Fig. 2), Fig. 7 was drawn. In this diagram only the region around the invariant

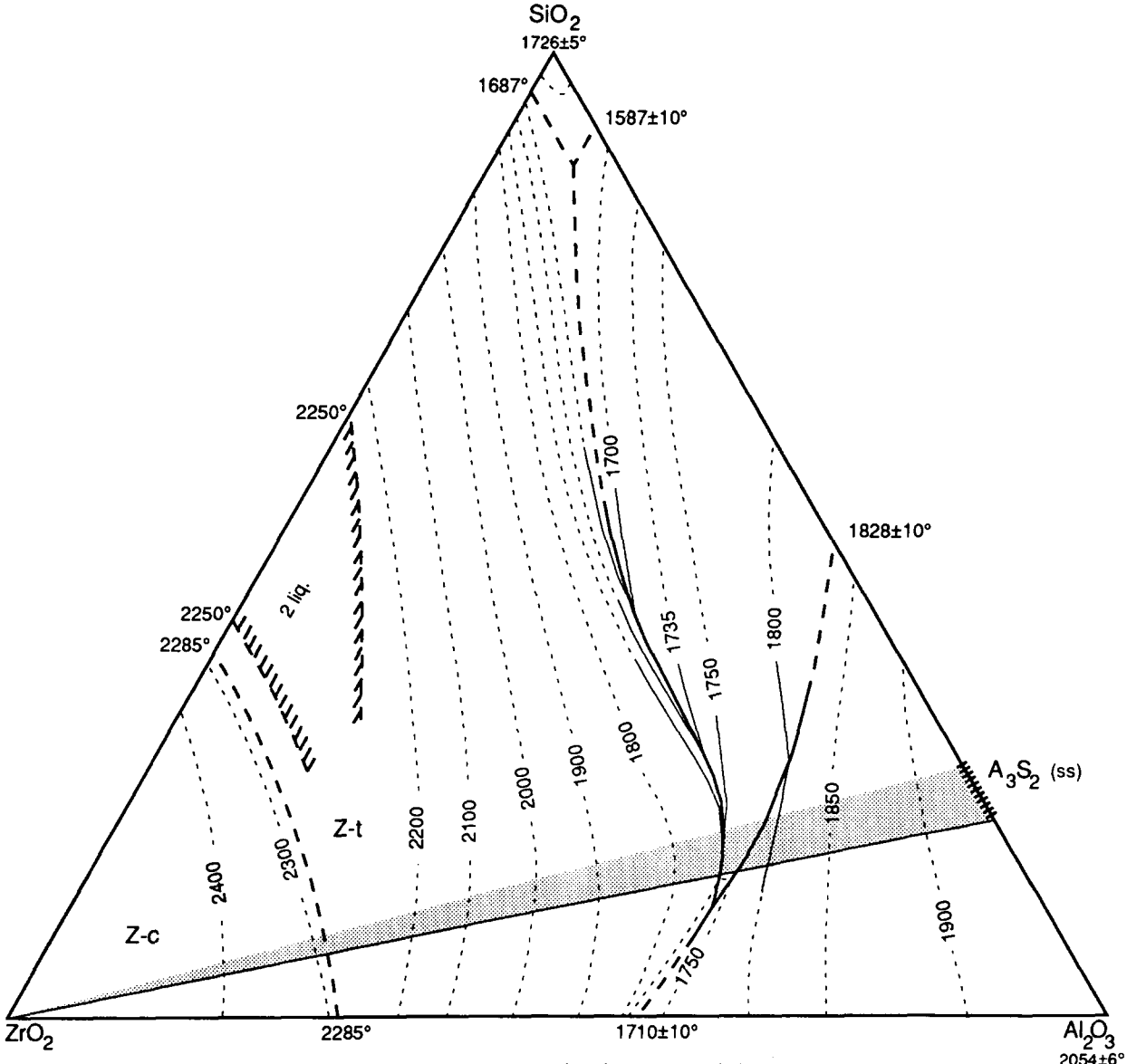

Fig. 7. Proposed phase diagram for the system Al_2O_3–ZrO_2–SiO_2.

point relating mullite, zirconia and alumina relates directly to the present work. All the rest is presumed, based on the binary systems and the diagram of Budnikov & Litvakovskii (Fig. 1), and is therefore drawn as dashed lines in Fig. 7. No information is available about the liquid immiscibility gap in the ternary system.

4 Conclusions

The main implications of the proposed diagram are: (1) the larger extent of the zirconia primary-phase field, down to significantly lower zirconia contents; (2) the higher alumina content of the mullite solid solution; (3) the ternary invariant point relating zirconia, alumina and mullite is of the eutectic type and occurs between 1700 and 1710°C, a temperature significantly lower than previously reported; and (4) the tentative composition of this ternary eutectic is *c.* $11SiO_2 + 58Al_2O_3 + 31ZrO_2$ (wt%), as opposed to $15{\cdot}6SiO_2 + 53{\cdot}2Al_2O_3 + 31{\cdot}2ZrO_2$ (wt%) indicated by the original Budnikov & Litvakovskii diagram.

Acknowledgements

The authors wish to thank C. M. Sá from CEMUP, Portugal, for the SEM work carried out. The financial support provided as grants abroad by CNPq and CAPES, Brazil, is gratefully acknowledged by M. C. Greca and J. V. Emiliano, respectively. This work was partially funded by INIC, Portugal.

References

1. Claussen, N., Rühle, M. & Heuer, A. H., Design of transformation toughened ceramics. In *Advances in Ceramics 12*, ed. A. H. Heuer & Manfred Rühle. The American Ceramic Society, Columbus, OH, 1983, pp. 325–51.
2. Evans, A. G. & Cannon, R. M., Toughening of brittle solids by martensitic transformations. *Acta Metall.*, **34**(5) (1986) 761–800.
3. Garvie, R. C., Goss, M. F., Marshall, S. & Urbani, C., Designing advanced refractories with monoclinic zirconia polycrystals. *Mat. Sci. Forum*, **34–36** (1988) 681–8.
4. Claussen, N. & Jahn, J., Mechanical properties of sintered, in-situ reacted mullite–zirconia composites. *J. Am. Ceram. Soc.*, **63**(3–4) (1980) 228–9.
5. Levin, E. M., Robbins, C. R. & McMurdie, H. F., In *Phase Diagrams for Ceramists*, ed. M. K. Reser. The American Ceramic Society, Columbus, OH, 1974, Figs 772, 2400 and 4377.
6. Pask, A., Phase equilibria in the Al_2O_3–SiO_2 system with emphasis on mullite. *Mat. Sci. Forum*, **34–36** (1988) 1–8.
7. Emiliano, J. V. & Segadães, A. M., Reaction-sintered mullite–zirconia composites—mechanism and properties. In *Zirconia 88*, ed. S. Meriani & C. Palmonari. Elsevier Applied Science, London, 1989, pp. 51–66.